Check for updates

ChemistryEurope

ChemistryEurope
Excellence in Chemistry Research Worldwide

RESEARCH ARTICLE OPEN ACCESS

Redox Modulation in Truxene-Based Phosphaalkenes Through Peripheral Substitution

Toma Bhowmick[1] | Rajesh Deka[1] | Ines Ballarini[2] | Andreas Orthaber[1]

[1]Department of Chemistry – Ångström Laboratories, Synthetic Molecular Chemistry, Uppsala, Sweden | [2]École National Graduate School of Engineering, Department of Materials and Chemistry, Caen, France

Correspondence: Andreas Orthaber (andreas.orthaber@kemi.uu.se)

Received: 26 May 2026 | **Revised:** 26 May 2026 | **Accepted:** 14 July 2026

Keywords: halogen | non-fullerene acceptor | phosphaalkene | redox potential | truxene

ABSTRACT

Peripheral functionalization of the polyaromatic hydrocarbon truxene with low-coordinate, low-valent ($\lambda^3\sigma^2$) phosphorus centers in the form of phosphaalkenes provides an effective strategy to induce deplanarization, improve solubility, and introduce pronounced π-acceptor character. Herein, we report the synthesis of halogenated truxene precursors bearing fluorine and bromine substituents and their stepwise transformation into mono-, di-, and triphosphaalkene derivatives. Progressive incorporation of phosphaalkene units leads to a systematic narrowing of the highest occupied molecular orbitals–lowest unoccupied molecular orbitals (LUMO) gap, as evidenced by bathochromic shifts in the low-energy absorption bands. Electrochemical studies reveal anodically shifted reduction potentials relative to the parent truxene phosphaalkenes, consistent with LUMO stabilization and enhanced electron-acceptor strength upon peripheral halogenation. Notably, the brominated derivatives reduce at milder potentials relative to their fluorinated counterparts, underscoring a nontrivial electronic modulation of the truxene framework that transcends simple electronegativity arguments. Density functional theory calculations corroborate these experimental trends and provide insight into the underlying structure–property relationships.

1 | Introduction

Truxene ($C_{27}H_{18}$) is a planar polyaromatic hydrocarbon (PAH) composed of three fluorene fragments fused via a central benzene ring (Figure 1A). First reported in 1894, it has since been extensively explored in various subfields of chemistry and materials science, with applications ranging from catalysis to organic light-harvesting materials [1–7]. The star-shaped molecule with C_3 symmetry is thermally stable and contains highly delocalized π-electrons, giving rise to its unique optoelectronic properties [8–10]. High solubility in common organic solvents achieved through alkylation of the fulvene core, the ability to take up multiple electrons, good absorption of light, and peripheral functionalization of the annulated flanking benzene rings to incorporate desired molecular properties have further established the utilization of truxene-based functional materials as small-molecule nonfullerene acceptors [11–14]. The exchange of the endocyclic carbon atom within the fulvene ring with heavier main-group elements—namely, Si, N, P, and O—introduces exceptional absorption behavior due to unique bonding situations exerted by the heteroatoms, enhancing donor characteristics (Figure 1B) [15–22]. Alternatively, the incorporation of electron-withdrawing fragments, such as C═O or C═N, on the bridgehead methylene positions significantly modulates the optical properties of this extended planar conjugated molecule, as well as introduces pronounced acceptor properties [23]. In 2016, Zhang and coworkers demonstrated that enforced contortion of the truxene core markedly amplifies electron-acceptor character. Oxidative di- and trimerization of substituted truxenones via elongated C═C linkers disrupt the coplanarity of the indene arms, generating twisted architectures whose deviation from planarity directly correlates with enhanced acceptor properties (Figure 1C) [24].

This is an open access article under the terms of the Creative Commons Attribution License, which permits use, distribution and reproduction in any medium, provided the original work is properly cited.

© 2026 The Author(s). *ChemistryEurope* published by Chemistry Europe and Wiley-VCH GmbH.

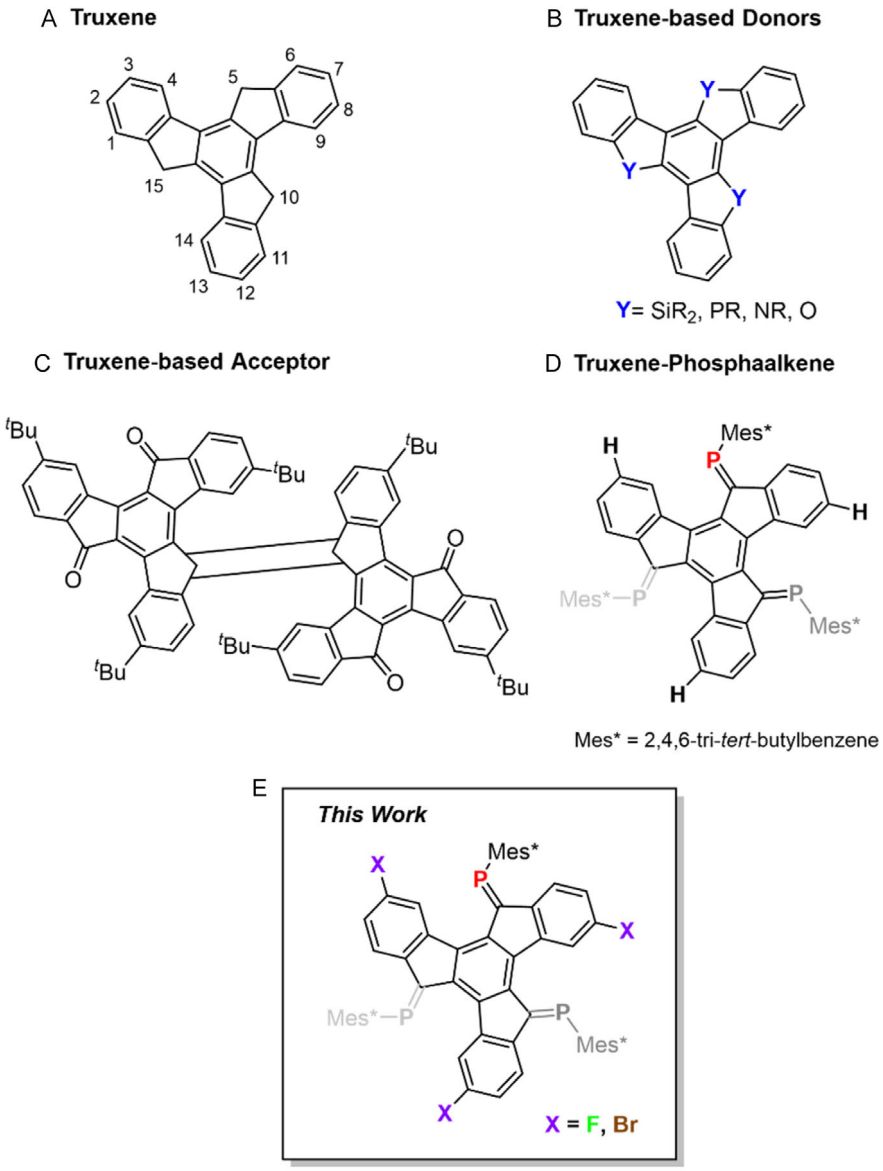

FIGURE 1 | Examples of truxene-functionalization: (A) truxene with numbering scheme, (B) truxene-based donors, (C) truxene-based acceptor, (D) truxene-phosphaalkene, **P*n*** ($n = 1, 2, 3$). (E) This work, $\mathbf{X_3P}n$ (where X = F, Br and $n = 1, 2, 3$) (Mes* = 2,4,6-tri-*tert*-butylbenzene).

Peripheral functionalization of PAHs with phosphaalkene (P═C) units offers a unique approach to incorporating main-group unsaturated fragments. This modification extends π-conjugation, selectively stabilizes the lowest unoccupied molecular orbitals (LUMO) level, and narrows the highest occupied molecular orbitals (HOMO)–LUMO gap, thereby imparting pronounced π-acceptor character to the molecular scaffold [25–30]. Our group has employed truxene as a core to bridge up to three exocyclic P═C units, yielding novel electron acceptors (**P1**-**P3**) that exhibit unique electronic and redox properties (Figure 1D) [31]. Interestingly, deplanarization, along with contributions from the bulky Mes* (2,4,6-tri-*tert*-butylbenzene) group, increased the solution processability of these small-molecule phosphaalkene acceptors. Sequential chemical reduction of these phosphaalkenes enabled the isolation of open-shell phosphorus-centered multiradical anions. This phenomenon is attributed to the inherent contortion of the π-framework upon phosphaalkene incorporation via mitigation of radical–radical interaction, which facilitates efficient charge accommodation and thereby highlights the potential of these systems as robust n-type acceptor materials [32].

Peripheral incorporation of electron-withdrawing substituents into extended π-conjugated frameworks represents a highly effective strategy for modulating the frontier molecular orbital energies and redox properties of organic semiconductor materials. In particular, halogen substitution has emerged as a powerful design principle for enhancing electron-acceptor character in PAHs and nonfullerene acceptors through stabilization of the LUMO energy level, modulation of intermolecular interactions, and tuning of charge-transport behavior [33–36]. Such approaches have brought about remarkable breakthroughs in modern organic electronic materials, where subtle electronic perturbations introduced by peripheral substitution directly govern optical absorption, reduction potentials, and overall semiconductor performance. Despite the extensive development of halogenated organic

27514765, 2026, 8, Downloaded from https://chemistry-europe.onlinelibrary.wiley.com/doi/10.1002/ceur.70340 by Uppsala University Library, Wiley Online Library on [13/08/2026]. See the Terms and Conditions (https://onlinelibrary.wiley.com/terms-and-conditions) on Wiley Online Library for rules of use; OA articles are governed by the applicable Creative Commons License

acceptors, analogous studies in unsaturated main-group functional materials remain largely unexplored.

Herein, we report the peripheral halogenation of truxene-based phosphaalkenes through the incorporation of fluorine and bromine substituents and present a systematic investigation of the substituent-dependent optical and electrochemical properties of the corresponding mono-, di-, and triphosphaalkenes. The study establishes direct correlations between halogen identity, frontier orbital modulation, and reduction behavior, revealing pronounced enhancement of acceptor character upon halogen substitution.

To the best of our knowledge, this represents the first systematic investigation of halogen substitution effects in low-coordinate phosphorus-containing π-acceptor materials and phosphaalkene-based conjugated systems. Beyond the synthesis of new molecular examples, the present work establishes broader structure–property relationships governing substituent-controlled tuning of phosphorus-based PAHs and provides general design principles for electronically tunable unsaturated main-group functional materials with relevance extending to the wider field of conjugated organic semiconductor research.

In our previous work, selective access to mono- and diphosphaalkenes was hampered by limited control over the formation of mono- and dianionic intermediates [31]. Introduction of *tert*-butyl substituents into the truxene core improved solubility and enabled selective monophosphaalkene formation (**P1^{tBu}**); however, increased electron density of the substituted scaffold precluded access to higher phosphaalkene homologues [37]. To overcome these limitations, we turned to electron-withdrawing substituents as a means to modulate the electronic structure of the truxene framework. With this rationale, halogen-substituted truxenes bearing fluorine or bromine atoms at the 3,8,13-positions were synthesized using a modified one-pot protocol, affording the targeted cores in excellent yields after simple purification (95%–96%) [24, 38].

Controlled lithiation of 3,8,13-trifluorotruxene, subsequent addition of Mes*PCl_2 to form respective chlorophosphines, followed by base-induced HCl elimination, afforded stepwise access to the mono-, di-, and triphosphaalkene derivatives, **F_3P1**-**F_3P3** (Scheme 1). Monolithiation proceeded cleanly to afford **F_3P1**, as evidenced by a single ^{31}P NMR resonance corresponding to the chlorophosphine intermediate upon addition of Mes*PCl_2. The isolation yielded 25% of pure product, and a characteristic $^{31}P\{^{19}F\}$ chemical shift at 269.4 ppm (C_6D_6) was observed. In contrast, lithiation with slightly more than two equivalents of ^{n}BuLi afforded **F_3P2** in 40% yield, along with a minor amount of **F_3P3** (8%). The $^{31}P\{^{19}F\}$ NMR spectrum displays two distinct resonances at 266.2 and 261.0 ppm, indicative of two inequivalent phosphorus centers. By comparison, **F_3P3** exhibits a $^{31}P\{^{19}F\}$ NMR signal at 262.0 ppm, consistent with three chemically equivalent phosphorus environments. A similar trend was observed in the trilithiation reaction, where **F_3P3** was isolated in 24% yield along with **F_3P2** as a byproduct (20%). The ^{31}P NMR spectra of all three fluorine-substituted phosphaalkenes are consistent with previously reported values (**P1–P3**).

In contrast, direct application of this protocol to the brominated truxene scaffold can lead to competing side reactions, most

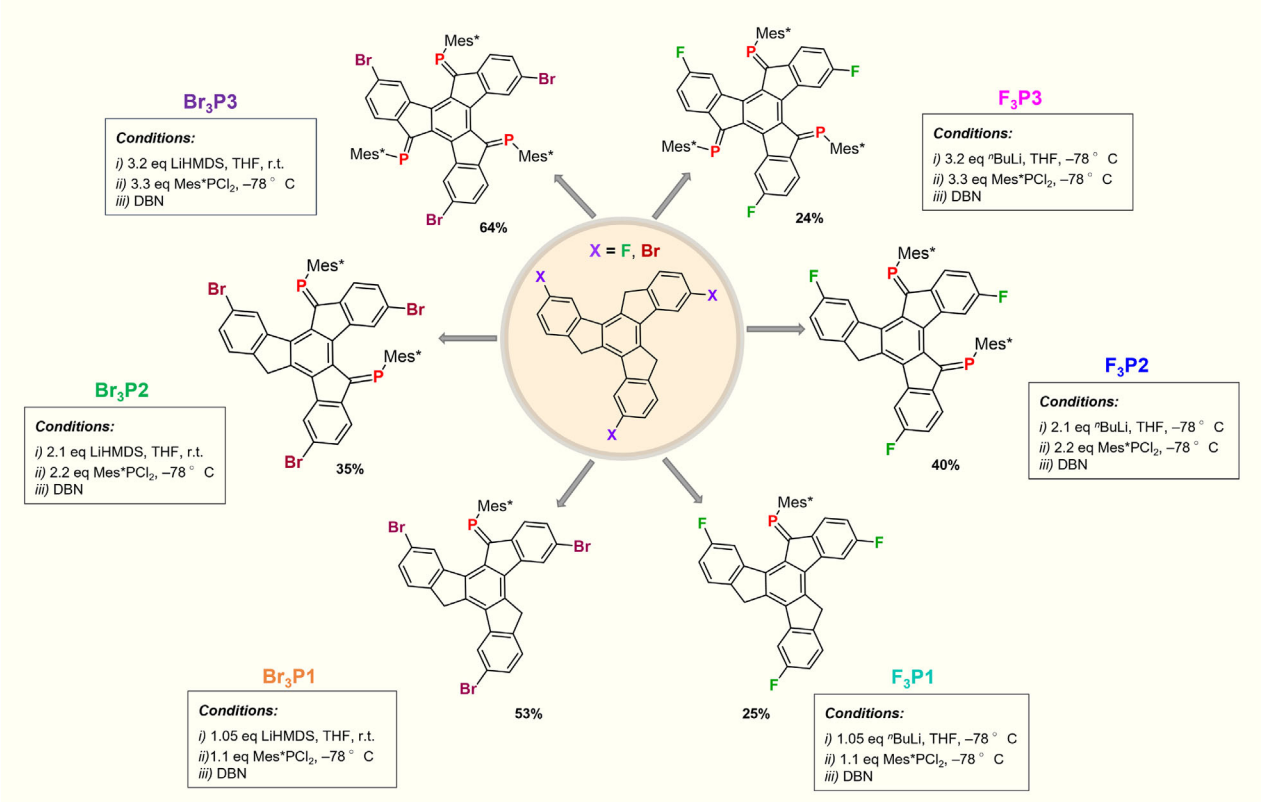

SCHEME 1 | Synthesis of 3,8,13-trifluorotruxene and of 3,8,13-tribromotruxene-based phoshphaalkenes.

27514765, 2026, 8, Downloaded from https://chemistry-europe.onlinelibrary.wiley.com/doi/10.1002/ceur.70340 by Uppsala University Library, Wiley Online Library on [13/08/2026]. See the Terms and Conditions (https://onlinelibrary.wiley.com/terms-and-conditions) on Wiley Online Library for rules of use; OA articles are governed by the applicable Creative Commons License

plausibly arising from dehalogenation and unintended alkylation pathways, as observed in our group's previous attempts (Figure S4). This limitation was circumvented by employing the mild, non-nucleophilic base, lithium bis(hexamethyldisilazide) (LiHMDS), which enabled selective deprotonation of the fulvene methylene positions while simultaneously stabilizing the resulting anionic intermediates. Notably, when present in excess, LiHMDS can also facilitate the formation of the final phosphaalkene product. Under these conditions, **Br_3P1**-**Br_3P3** were obtained with good selectivity, with the triphosphaalkene, **Br_3P3** (64%) isolated in the highest yield of the series. The monophosphaalkene, **Br_3P1**, was obtained in 53% yield, displaying a characteristic $^{31}P\{^1H\}$ resonance at 278.3 ppm in $CDCl_3$ (Scheme 1). Stepwise incorporation of additional phosphaalkene units afforded the diphosphaalkene, **Br_3P2**, in 35% yield, with only trace amounts of **Br_3P1** detected, and is characterized by two $^{31}P\{^1H\}$ signals at 273.6 and 267.3 ppm ($CDCl_3$). The triphosphaalkene **Br_3P3** showcases a single $^{31}P\{^1H\}$ resonance at 267.3 ppm in C_6D_6, and only trace quantities of **Br_3P1** and **Br_3P2** were formed during the synthesis. Compared to the corresponding trifluorotruxene-derived phosphaalkenes, both yields and selectivities are markedly improved, a trend attributed to the prolonged room-temperature deprotonation enabled by LiHMDS, which facilitates efficient formation and stabilization of the key anionic intermediates while suppressing competing side reactions.

Single-crystal X-ray diffraction analysis provided detailed insight into the solid-state structures of the phosphaalkenes. Single crystals of compounds **F_3P1** and **F_3P2** are obtained through slow evaporation from diethyl ether. Compound **F_3P1** crystallizes in the triclinic space group, *P*−1, with P(1)═C distance 1.692(2) Å, and C—P═C angle 104.0(1)°, which is the expected range for phosphaalkenes (Figure 2) [39]. However, unlike the unsubstituted monophosphaalkene, **P1**, **F_3P1** has a P—C bond configuration *trans* to the central phenyl ring of the truxene core, which is in line with the observation with **P1^{tBu}** [37]. Out-of-plane contortion of the indane arm containing the P═C is observed, while no π–π interaction is observed in solid-state packing. Compound **F_3P2** crystallizes in the monoclinic space group, $P2_1/c$, where both P═C-containing indane arms exhibit significant deviation from planarity, while the unsubstituted fulvene core remains planar. P—C double bond distances are within the expected range with P(1)═C 1.693(3) Å, P(2)═C 1.698(2) Å, with C—P═C angles 105.8(1)° and 105.5(1)° (Table 1). Despite multiple attempts, satisfactory crystals of **F_3P3** were not acquired to report solid-state parameters. Regardless, based on a low-resolution structure determination, the identity of the compound and an *up*, *up*, *down* configuration of the P═C units was clearly established (Figure S2). Notably, **F_3P3** exhibits slow degradation under ambient conditions over time. Evidence for this behavior was obtained from single-crystal X-ray diffraction analysis of crystals isolated during a crystallization attempt, which showed partial hydrolysis of the phosphaalkene units (Figure S3).

Single crystals of compounds **Br_3P2** and **Br_3P3** are obtained through slow diffusion of pentane in a concentrated toluene mixture. The brominated derivatives exhibit similar P═C bond metrics but display more pronounced deviations from planarity. Compound **Br_3P2** crystallizes in the triclinic space group *P*−1. P—C double bond distances are within the expected range, with P(1)═C 1.696(2) Å, P(2)═C 1.699(2) Å, with C—P═C angles 105.1(1)° and 103.0(1)° (Figure 2). Compound **Br_3P3** exhibits a monoclinic space group $P2_1/c$ with four molecules in the unit cell. The P═C bond distances follow a similar trend with P(1)═C 1.693(3) Å, P(2)═C 1.695(3) Å and P(3)═C 1.695(2) Å, with C—P═C angles 103.7(1)°, 103.0(1)°, and 104.6(1)°. The P═C containing indane arms are twisted out-of-plane from the central phenyl ring, and prevail an *up, up, up* configuration with respect to the central arene of the truxene core, which is quite different from **F_3P3**. Intermolecular stacking is observed for this highly symmetric moiety, with two molecules sitting on top of each other, forming a cavity with a centroid–centroid distance of 6.1 Å along the central phenyl ring (Figure S5).

The UV–vis absorption spectra of the phosphaalkenes, recorded in dichloromethane (DCM) (Figure 3), closely resemble those of the corresponding unsubstituted analogues. The monophosphaalkene, **F_3P1**, exhibits a π→π* absorption maximum at

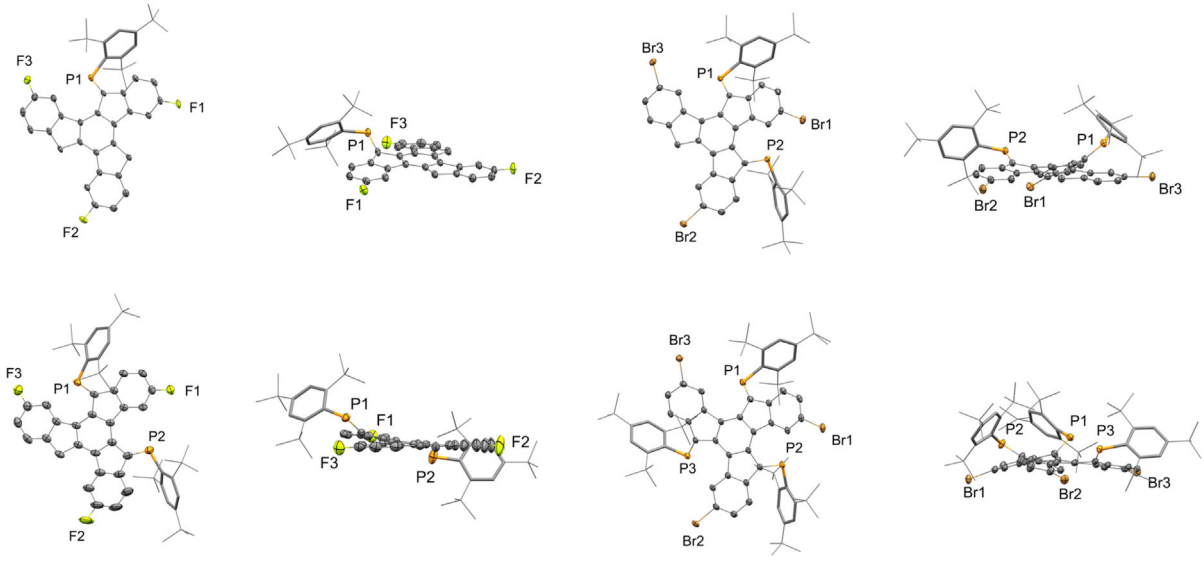

FIGURE 2 | Solid-state structures (top-view vs. side-view) of phosphaalkenes: *top left*) **F_3P1**, *bottom left*) **F_3P2**, *top right*) **Br_3P2**, *bottom right*) **Br_3P3**.

27514765, 2026, 8, Downloaded from https://chemistry-europe.onlinelibrary.wiley.com/doi/10.1002/ceur.70340 by Uppsala University Library, Wiley Online Library on [13/08/2026]. See the Terms and Conditions (https://onlinelibrary.wiley.com/terms-and-conditions) on Wiley Online Library for rules of use; OA articles are governed by the applicable Creative Commons License

TABLE 1 | Redox potentials and UV–vis absorption spectra of the phosphaalkenes, along with their previously reported unsubstituted cogeners [31].

Entry	P1	P2	P3	F_3P1	F_3P2	F_3P3	Br_3P1	Br_3P2	Br_3P3
$E_{1/2}$ (V vs. Fc/Fc^+)	−1.92	−1.77	−1.89	−1.61	−1.49	−1.47	−1.43	−1.43	−1.06
		−2.20	−2.23		−1.92	−1.91		−1.86	−1.45
			−2.67			−2.33			−2.40[a]
λ_{max} (nm)	317	325	330	319	328	332	325	332	341
	—	—	390	—	368	395	—	374	399
	428	435	452	420	424	445	426	434	455

[a]Irreversible redox event.

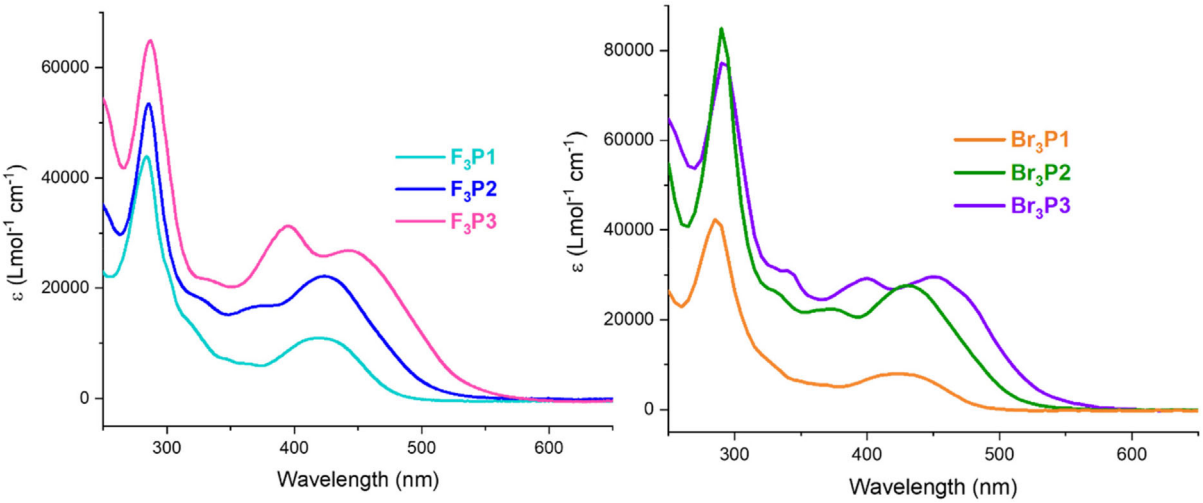

FIGURE 3 | UV–vis spectra recorded in DCM (5 μM) *left*) **F_3P1-F_3P3**, *right*) **Br_3P1-Br_3P3**.

420 nm, representing an ∼8 nm hypsochromic shift relative to **P1**. In a similar manner, **F_3P2** (λ_{max} = 424 nm) and **F_3P3** (λ_{max} = 445 nm) display blue shifts of ≈7–10 nm compared to their unsubstituted counterparts, **P2** and **P3** (Table 1). This observation is consistent with concomitant stabilization of both the HOMO and LUMO energy levels, resulting in a slight widening of the HOMO–LUMO gap upon peripheral fluorination of the truxene core (Table S4). The brominated derivatives follow analogous trends: **Br_3P1** shows a π→π* transition at 426 nm, comparable to **P1**, while **Br_3P2** (λ_{max} = 434 nm) and **Br_3P3** (λ_{max} = 455 nm) are bathochromically shifted by ca. 10 nm relative to the fluorinated analogues. Overall, the close correspondence of the absorption maxima to those of the unsubstituted phosphaalkenes indicates that bromine substitution exerts only a marginal effect on the frontier molecular orbital splitting.

Cyclic voltammetry (CV) measurements were carried out to investigate the redox behavior of the six newly synthesized phosphaalkenes. The CV profiles of **F_3P1-F_3P3** closely resemble those of previously reported unsubstituted analogues (**P1**-**P3**), each displaying one, two, and three reversible reduction processes within a narrow potential range [31]. The monophosphaalkene **F_3P1** exhibits a single reversible reduction at $E_{1/2}$ = −1.61 V versus Fc/Fc^+, representing an anodic shift of ≈300 mV relative to **P1** ($E_{1/2}$ = −1.89 V vs. Fc/Fc^+) (Figure 4, Table 1). This pronounced shift can be attributed to the strong electron-withdrawing influence of the fluorine atoms on the truxene core, which reduces π-electron density within the conjugated system and effectively lowers the LUMO level, thereby modulating the molecule's overall electronic structure (vide infra). This trend continues across the series: **F_3P2** shows two reversible reductions at −1.49 and −1.92 V (vs. Fc/Fc^+), while **F_3P3** displays three reversible reduction waves at −1.47, −1.91, and −2.33 V (vs. Fc/Fc^+). The first reduction potential of **F_3P3** is anodically shifted by ≈400 mV relative to unsubstituted triphosphaalkene, **P3**, with the second and third reductions shifted by around 300 mV (Table 1). The close correspondence of the first two redox events of **F_3P3** with those of **F_3P2** suggests that the maximal electronic influence of the fluorine substituents and the incorporated phosphaalkene units is already reached at the diphosphaalkene stage.

In contrast, the bromine-substituted derivatives exhibit distinctly different electrochemical behavior. **Br_3P1** undergoes a single reversible reduction at −1.43 V (vs. Fc/Fc^+), which is significantly milder than even the first reduction observed for **F_3P3** (Figure 4). **Br_3P2** displays two reversible reduction processes at −1.43 and −1.86 V (vs. Fc/Fc^+). Interestingly, only two reversible reductions are observed for **Br_3P3** at −1.06 and −1.45 V (vs. Fc/Fc^+), while a third, irreversible event occurs at more negative potentials (−2.40 V vs. Fc/Fc^+, Figure S1). The latter feature is likely attributed to in situ debromination (partial) of the truxene core, followed by protonation during the reverse scan (Figure S1). This phenomenon is consistent with the electrochemical debromination behavior reported for brominated aromatic compounds, as

27514765, 2026, 8, Downloaded from https://chemistry-europe.onlinelibrary.wiley.com/doi/10.1002/ceur.70340 by Uppsala University Library, Wiley Online Library on [13/08/2026]. See the Terms and Conditions (https://onlinelibrary.wiley.com/terms-and-conditions) on Wiley Online Library for rules of use; OA articles are governed by the applicable Creative Commons License

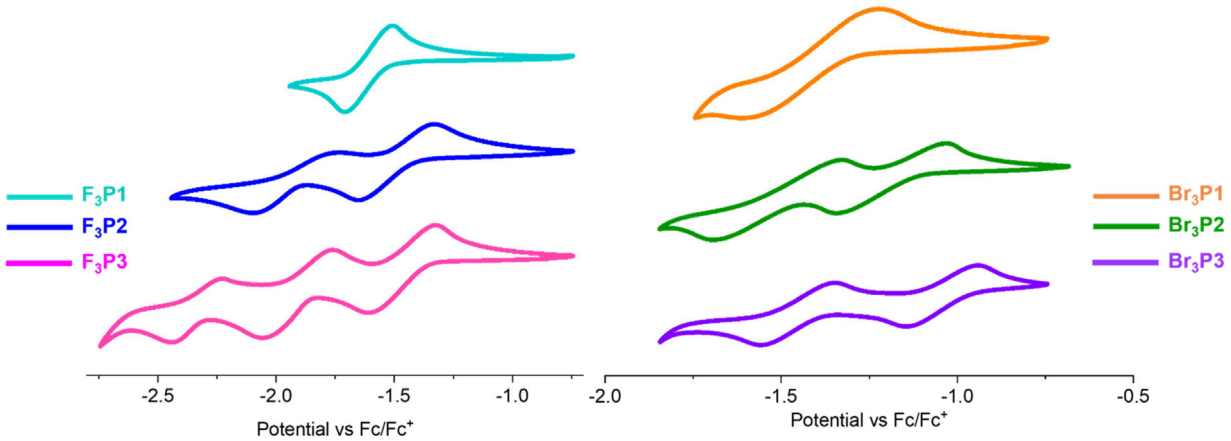

FIGURE 4 | Cyclic voltammetry recorded at 100 mVs^{-1} scan rate in THF (2 mM) with $TBAPF_6$ as the supporting electrolyte (0.1 M) *left*) **F_3P1-F_3P3**, *right*) **Br_3P1-Br_3P3**.

the observed potential window closely matches those associated with electrochemical C—Br bond activation [40–42]. Notably, all six phosphaalkenes undergo reduction at substantially milder potentials than **P3**, with **Br_3P3** exhibiting the most pronounced shift, reaching reduction potentials up to 800 mV less negative than those of **P3**. Such remarkable modulation highlights the exceptional degree of electronic tuning and enhancement of π-acceptor character upon halogen functionalization of the conjugated framework. Intriguingly, the brominated derivatives undergo reduction at even milder potentials than their fluorinated congeners, demonstrating that halogen-induced modulation of the truxene electronic structure is governed not solely by electronegativity, but rather by a delicate balance between σ-inductive stabilization and π-resonance contributions. These effects are intrinsically dependent on both the identity and size of the halogen substituent. Thus, the anodic shift in reduction potential upon halogenation arises from the combined electronic and structural consequences of F versus Br.

Density functional theory (DFT) calculations at the M06-2X/6-311G** level support the experimental observations. In all cases, the HOMOs correspond to delocalized π-bonding orbitals, extending over the truxene framework and the phosphaalkene bond, with substantial halogen participation, whereas the lowest unoccupied molecular orbitals (LUMOs) are dominated by antibonding π*-orbitals and exhibit only minor halogen contribution (Figure S8). The more pronounced stabilization of the frontier molecular orbitals—particularly the LUMOs in the brominated derivatives relative to their fluorinated analogues, accounts for their systematically milder reduction potentials (Figure 5, Figure S6).

In contrast, the closely resembling low-energy absorption maxima observed in spectroscopic studies across both halogen series arise from a near-uniform stabilization of the HOMOs: upon incorporation of two and three phosphaalkene units, these orbitals undergo systematic destabilization, giving rise to observed bathochromic shifts in the absorption spectra, in agreement with previous reports [31]. Notably, DFT calculations reveal that the HOMOs of the brominated derivatives display a substantially greater contribution from the bromine atoms than the corresponding fluorine contribution in the fluorinated analogues, underscoring the pronounced involvement of bromine in shaping the frontier

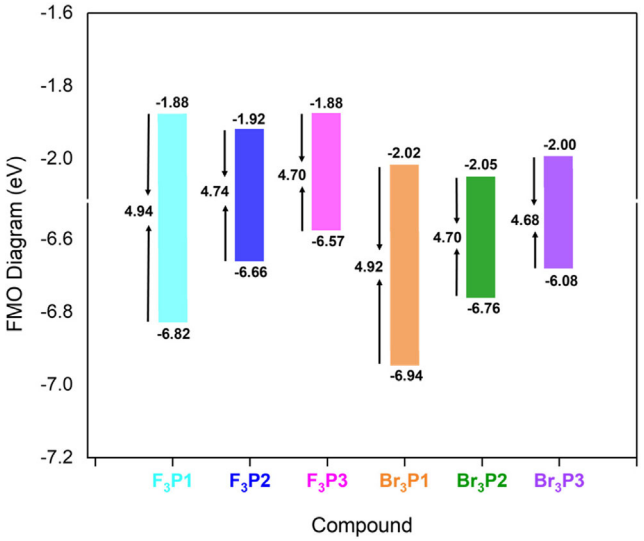

FIGURE 5 | Calculated HOMO–LUMO energies and band gaps across the phosphaalkenes.

molecular orbitals, which is consistently reflected in their redox behavior (Figure S8). Overall, these results demonstrate that the optoelectronic properties of truxene-based phosphaalkenes are governed by a subtle interplay of halogen electronegativity, polarizability, structural distortion (Figure S7), and delocalization effects imparted by peripheral halogen substitution.

2 | Conclusion

Halogen substitution is a well-established strategy for modulating the HOMO–LUMO gap in PAHs. In this work, we introduce a dual-modulation strategy that combines peripheral halogenation (F, Br) with phosphaalkene incorporation into the truxene scaffold. Phosphaalkene insertion enables controlled extension of effective conjugation while inducing predictable distortion of the fulvene core, thereby enforcing nonplanarity within the otherwise planar PAH framework. These structural deviations are further accentuated by the size differences of the incorporated

27514765, 2026, 8, Downloaded from https://chemistry-europe.onlinelibrary.wiley.com/doi/10.1002/ceur.70340 by Uppsala University Library, Wiley Online Library on [13/08/2026]. See the Terms and Conditions (https://onlinelibrary.wiley.com/terms-and-conditions) on Wiley Online Library for rules of use; OA articles are governed by the applicable Creative Commons License

halogens. Together, the structural and electronic perturbations establish two handles for tuning contortion and frontier molecular orbital energies.

Electrochemical studies reveal that all six halogenated phosphaalkenes are reduced at significantly milder potentials compared to their unsubstituted counterparts, underscoring the enhancement of π-acceptor character upon peripheral halogenation. Notably, the brominated derivatives exhibit even milder reduction potentials than the corresponding fluorinated systems, an effect attributed to increased polarizability of their frontier molecular orbitals. DFT calculations support the experimental findings. These results establish halogen substitution and phosphaalkene incorporation as design principles for engineering electronically tunable, contorted phosphorus-embedded PAHs. Importantly, although the brominated derivatives, particularly the triphosphaalkene, undergo reduction at substantially milder potentials than their fluorinated counterparts, peripheral fluorination offers a distinct advantage by enabling access to a significantly broader electrochemical window while still supporting three fully reversible reduction events without inducing decomposition or irreversible degradation of the π-conjugated framework. These observations further highlight the subtle yet important role of halogen substitution in balancing reductive accessibility with electrochemical robustness in phosphorus-containing π-functional materials. Ongoing efforts are directed towards leveraging the halogens as synthetic handles for subsequent functionalization, positioning these scaffolds as versatile starting points for expanding the electronic and chemical landscape of main-group-based PAHs.

Acknowledgements

The authors thank the Swedish Research Council (A. O., T.B: project 2017−03727, 2021−03658), Olle Engkvists Stiftelse (R.D.), and the Wenner-Gren Foundation (R.D.) for their financial support. We are grateful to the ERASMUS+ (2021−2027) program, enabling the international student exchanges (I.B.). The computations were enabled by resources in project UPPMAX-2025-2-386 provided by Uppsala University at UPPMAX.

Funding

This study was supported by Vetenskapsrådet (2017-03727 and 2021-03658), Olle Engkvists Stiftelse, Wenner-Gren Stiftelserna, Erasmus+, Uppsala Multidisciplinary Center for Advanced Computational Science.

Conflicts of Interest

The authors declare no conflicts of interest.

Data Availability Statement

The data that supports the findings of this study are available in the supplementary material of this article.

References

1. F. S. Kipping, "XXIX. The Formation of the Hydrocarbon 'Truxene' From Phenylpropionic Acid, and From Hydrindone," *Journal of the Chemical Society, Transactions* 65 (1894): 269–290.

2. F. Goubard and F. Dumur, "Truxene: A Promising Scaffold for Future Materials," *RSC Advances* 5 (2015): 3521–3551.

3. S. A. Wagay, I. A. Rather, and R. Ali, "Functionalized Truxene Scaffold: A Promising Advanced Organic Material for Digital Era," *ChemistrySelect* 4 (2019): 12272–12288.

4. K. Shi, J.-Y. Wang, and J. Pei, "π-Conjugated Aromatics Based on Truxene: Synthesis, Self-Assembly, and Applications," *Chemical Record* 15 (2015): 52–72.

5. J. Guadalupe, A. M. Ray, E. M. Maya, B. Gómez-Lor, and M. Iglesias, "Truxene-Based Porous Polymers: From Synthesis to Catalytic Activity," *Polymer Chemistry* 9 (2018): 4585–4595.

6. A. Brnovic, G. Kumar, M. Axelsson, et al., "Triplet States Enable Efficient Photocatalytic Hydrogen Evolution in Star-Shaped Truxene-Based Nanoparticles," *Chemical Science* 17 (2026): 7525–7532, https://doi.org/10.1039/D5SC09380E.

7. C. Yao, Y. Yu, X. Yang, et al., "Effective Blocking of the Molecular Aggregation of Novel Truxene-Based Emitters With Spirobifluorene and Electron-Donating Moieties for Furnishing Highly Efficient Non-Doped Blue-Emitting OLEDs," *Journal of Materials Chemistry C* 3 (2015): 5783–5794.

8. J. Huang, B. Xu, J.-H. Su, C. H. Chen, and H. Tian, "Efficient Blue Lighting Materials Based on Truxene-Cored Anthracene Derivatives for Electroluminescent Devices," *Tetrahedron* 66 (2010): 7577–7582.

9. B. Kaur, D. Moghe, A. Dey, D. Kabra, and J. Jacob, "Solution Processable Truxene Based Blue Emitters: Synthesis, Characterization and Electroluminescence Studies," *Journal of Luminescence* 196 (2018): 511–519.

10. Y. Guo, H. S. Torchon, Y. Zhu, et al., "Stepwise Deprotonation of Truxene: Structures, Metal Complexation, and Charge-Dependent Optical Properties," *Chemical Science* 14 (2023): 13219–13227.

11. K. Lin, B. Xie, Z. Wang, et al., "Star-Shaped Electron Acceptors Containing a Truxene Core for Non-Fullerene Solar Cells," *Organic Electronics* 52 (2018): 42–50.

12. K. Lin, W. Du, S. Shen, et al., "Truxene-Centered Electron Acceptors for Non-Fullerene Solar Cells: Alkyl Chain and Branched Arm Engineering," *International Journal of Molecular Sciences* 23 (2022): 10402.

13. P. Li, F. Wu, Y. Fang, et al., "Truxene π-Expanded BODIPY Star-Shaped Molecules as Acceptors for Non-Fullerene Solar Cells With Over 13% Efficiency," *ACS Applied Energy Materials* 5 (2022): 2279–2289.

14. R. Ali, S. Alvi, and M. Sattar, "Applications of Truxene and Its Congeners in Solar Cells: A Recent Update," *Polycyclic Aromatic Compounds* 44 (2024): 7197–7216.

15. T. Ogaki, E. Ohta, Y. Oda, et al., "Intramolecular Triple Cyclization Strategy for Sila- and Oxa-Analogues of Truxene With Long-Lived Phosphorescence," *Asian Journal of Organic Chemistry* 6 (2017): 290–296.

16. T. Kojima, S. Furukawa, H. Tsuji, and E. Nakamura, "Synthesis of Triphosphatruxene via Sextuple Aromatic Nucleophilic Substitution and Simple Isolation of Stereoisomers," *Chemistry Letters* 43 (2014): 676–677.

17. T. Techajaroonjit, S. Namuangruk, N. Prachumrak, V. Promarak, M. Sukwattanasinitt, and P. Rashatasakhon, "Synthesis, Characterization, and Hole-Transporting Properties of Pyrenyl N -Substituted Triazatruxenes," *RSC Advances* 6 (2016): 56392–56398.

18. A. Tripathi and C. Prabhakar, "Optoelectronic and Charge-Transport Properties of Truxene, Isotruxene, and Its Heteroatomic (N, O, Si, and S) Analogs: A DFT Study," *Journal of Physical Organic Chemistry* 32 (2019): e3944.

19. B. Gómez-Lor, G. Hennrich, B. Alonso, A. Monge, E. Gutierrez-Puebla, and A. M. Echavarren, "A Redox-Active C_3-Symmetric Triindole-Based Triazacyclophane," *Angewandte Chemie International Edition* 45 (2006): 4491–4494.

20. E. M. García-Frutos, B. Gómez-Lor, Á. Monge, E. Gutiérrez-Puebla, I. Alkorta, and J. Elguero, "Synthesis and Preferred All-Syn Conformation

27514765, 2026, 8, Downloaded from https://chemistry-europe.onlinelibrary.wiley.com/doi/10.1002/ceur.70340 by Uppsala University Library, Wiley Online Library on [13/08/2026]. See the Terms and Conditions (https://onlinelibrary.wiley.com/terms-and-conditions) on Wiley Online Library for rules of use; OA articles are governed by the applicable Creative Commons License

of C_3-Symmetrical N-(Hetero)arylmethyl Triindoles," *Chemistry – A European Journal* 14 (2008): 8555–8561.

21. Y. Che, M. R. Niazi, Q. Chan, et al., "Design of Furan-Based Acceptors for Organic Photovoltaics," *Angewandte Chemie International Edition* 62 (2023): e202309003.

22. V. Bocchi and G. Palla, "Synthesis and Characterization of New Indole Trimers and Tetramers," *Tetrahedron* 42 (1986): 5019–5024.

23. K. Jacob, J. Y. Becker, A. Ellern, and V. Khodorkovsky, "Synthesis of Novel Truxenequinone Based Electron Acceptors," *Tetrahedron Letters* 40 (1999): 8625–8628.

24. G. Zhang, V. Lami, F. Rominger, Y. Vaynzof, and M. Mastalerz, "Rigid Conjugated Twisted Truxene Dimers and Trimers as Electron Acceptors," *Angewandte Chemie* 128 (2016): 4045–4049.

25. A. El Nahhas, M. A. Shameem, P. Chabera, J. Uhlig, and A. Orthaber, "Synthesis and Characterization of Cyclopentadithiophene Heterofulvenes: Design Tools for Light-Activated Processes," *Chemistry – A European Journal* 23 (2017): 5673–5677.

26. J. P. Green, D. Morales Salazar, A. K. Gupta, and A. Orthaber, "Golden Age of Fluorenylidene Phosphaalkenes–Synthesis, Structures, and Optical Properties of Heteroaromatic Derivatives and Their Gold Complexes," *The Journal of Organic Chemistry* 85 (2020): 14619–14626.

27. S. Ito, H. Sugiyama, and M. Yoshifuji, "Isolation of a Kinetically Stabilized 1,3,6-Triphosphafulvene," *Angewandte Chemie International Edition* 39 (2000): 2781–2783.

28. G. Tan, S. Li, S. Chen, Y. Sui, Y. Zhao, and X. Wang, "Isolable Diphosphorus-Centered Radical Anion and Diradical Dianion," *Journal of the American Chemical Society* 138 (2016): 6735–6738.

29. G. Märkl and K. M. Raab, "Phosphapentafulvene," *Tetrahedron Letters* 30 (1989): 1077–1080.

30. R. Deka, T. Bhowmick, and A. Orthaber, "Expect the Unexpected – Li^+ Migration Governing the Substitution of 7 H-Benzo[De]anthracene With Main-Group Fragments," *Chemical Communications* 62 (2026): 1900–1904.

31. M. A. Shameem, J. A. L. Wells, A. K. Gupta, and A. Orthaber, "One, Two Three – Phosphaalkene Decoration Tailoring Solubility and Electronic Properties of Truxene-Based Electron Acceptors," *Chemistry – A European Journal* 29 (2023): e202300563.

32. M. A. Ansari, R. Deka, A. Thapper, and A. Orthaber, "Expanding the Landscape of Phosphorous-Based Open Shell Species: Stable Mono-, Di-, and Trianionic Radicals Based on a Contorted Triphosphaalkene," *Angewandte Chemie International Edition* 64 (2025): e202415684.

33. F. Benlakhdar, M. A. Ghebouli, M. Fatmi, et al., "Effect of Halogen Substitution on the Electronic and Optical Behavior of $C_{10}H_{10}X_2O_2$(X = F, Cl, Br and I) Organic Semiconductors," *Scientific Reports* 15 (2025): 25891.

34. S. Roosta, M. Elstner, and W. Xie, "Effect of Halogen Substituents on Charge Transport Properties of n-Type Organic Semiconductors: A Theoretical Study," *The Journal of Physical Chemistry A* 128 (2024): 8878–8885.

35. Y.-B. Wang, Y.-J. Xue, C.-M. Hung, et al., "Effect of Halogen/Chalcogen Substitution on the Dielectric Constant of Asymmetric Acceptor Alloy to Improve the Efficiency and Stability of Inverted Organic Photovoltaics," *Chemical Science* 16 (2025): 17391–17407.

36. S. Lu, F. Li, K. Zhang, et al., "Halogenation on Terminal Groups of ITIC Based Electron Acceptors as an Effective Strategy for Efficient Polymer Solar Cells," *Solar Energy* 195 (2020): 429–435.

37. T. Bhowmick, J. A. L. Wells, M. Asif Ansari, J. D. Steen, S. Crespi, and A. Orthaber, "Reversible Metal-Mediated Molecular Switching of a Phosphaethene Polyaromatic Hydrocarbon," *Chemistry – A European Journal* 31 (2025): e202403974.

38. N. Méndez-Gil, S. Gámez-Valenzuela, M. Echeverri, et al., "Donor-Acceptor Truxene-Based Porous Polymers: Synthesis, Optoelectronic Characterization and Defense-Related Applications," *Advanced Functional Materials* 34 (2024): 2316754.

39. R. Deka, J. D. Steen, M. F. Hilbers, et al., "Probing the Hidden Photoisomerization of a Symmetric Phosphaalkene Switch," *Angewandte Chemie International Edition* 64 (2025): e202419943.

40. J. K. LaPier, Y.-J. Liu, J. F. King, T. Béguerie, A. Nzihou, and W. A. Mitch, "Electrochemical Debromination of Brominated Aromatic Flame Retardants Using Activated Carbon-Based Cathodes," *Environmental Science & Technology* 60 (2026): 1346–1356.

41. S. Neukermans, F. Vorobjov, T. Kenis, R. De Wolf, J. Hereijgers, and T. Breugelmans, "Electrochemical Reduction of Halogenated Aromatic Compounds at Metal Cathodes in Acetonitrile," *Electrochimica Acta* 332 (2020): 135484.

42. C. Durante, A. A. Isse, F. Todesco, and A. Gennaro, "Electrocatalytic Activation of Aromatic Carbon-Bromine Bonds Toward Carboxylation at Silver and Copper Cathodes," *Journal of the Electrochemical Society* 160 (2013): G3073.

Supporting Information

Additional supporting information can be found online in the Supporting Information section. The authors have cited additional references within the Supporting Information [24, 38]

27514765, 2026, 8, Downloaded from https://chemistry-europe.onlinelibrary.wiley.com/doi/10.1002/ceur.70340 by Uppsala University Library, Wiley Online Library on [13/08/2026]. See the Terms and Conditions (https://onlinelibrary.wiley.com/terms-and-conditions) on Wiley Online Library for rules of use; OA articles are governed by the applicable Creative Commons License